Low-density neutron matter

Alexandros Gezerlis[1,2,3] and J. Carlson[1]
[1]*Theoretical Division, Los Alamos National Laboratory, Los Alamos, New Mexico 87545, USA*
[2]*Department of Physics, University of Illinois at Urbana-Champaign, Urbana, Illinois 61801, USA*
[3]*Department of Physics, University of Washington, Seattle, Washington, 98195, USA*
(Received 19 November 2009; published 17 February 2010)

The properties of low-density neutron matter are important for the understanding of neutron star crusts and the exterior of large neutron-rich nuclei. We examine various properties of dilute neutron matter using quantum Monte Carlo methods, with s- and p-wave terms in the interaction. Our results provide a smooth evolution of the equation of state and pairing gap from extremely small densities, where analytic expressions are available, up to the strongly interacting regime probed experimentally and described theoretically in cold atomic systems, where $k_F \approx 0.5$ fm^{-1} and the pairing gap becomes of the order of magnitude of the Fermi energy. We also present results for the momentum distribution and pair distributions, displaying the same evolution from weak to strong coupling. Combined with previous quantum Monte Carlo and other calculations at moderate densities, these results provide strong constraints on the neutron matter equation of state up to saturation densities.

DOI: 10.1103/PhysRevC.81.025803 PACS number(s): 21.65.−f, 03.75.Ss, 05.30.Fk, 26.60.−c

I. INTRODUCTION

The equation of state and the pairing gap of neutron matter at low densities are important for describing the properties of the inner crusts of neutron stars and provide significant constraints for density-functional theories of large neutron-rich nuclei. Equation of state results at larger densities ($\rho \geqslant 0.04$ fm^{-3}) have been used for some time to constrain Skyrme and other density functional approaches to large nuclei [1,2]. More recently, the density-dependence of the $^1S_0$ gap in low-density neutron matter has been used to constrain Skyrme-Hartree-Fock-Bogoliubov treatments and especially their description of neutron-rich nuclei [3]. At extremely low densities the equation of state and pairing gap can be expressed as analytically known functions of $(k_F a)$, the product of the Fermi momentum and the neutron-neutron scattering length. Our results provide a smooth connection between these analytic results and previous calculations of neutron matter at larger densities, where the gaps become smaller and the superfluid properties are less relevant to the equation of state.

The properties of low-density neutron matter are particularly important for describing the inner crust of a neutron star, which is composed of a lattice of neutron-rich nuclei along with a gas of neutrons and electrons. The neutron gas at low densities is expected to be superfluid; the evolution of the equation of state and the pairing gap will impact the static and dynamic properties of the inner crust of the neutron star. A cold neutron star will have a temperature from 10^6 K to 10^9 K ($\sim$0.1 keV to 0.1 MeV); hence the low-density neutron gas is superfluid because the critical temperature is expected to be larger, approximately 10^{10} K ($\sim$1 MeV). The most basic aspects of a superfluid gas embedded in a lattice of nuclei are described by zero-temperature infinite pure neutron matter. Corrections to this picture include gradient terms in the density induced by the ionic lattice. While these corrections are also important for density-functional theories of nuclei, we leave their study to future investigations.

Superfluidity in neutron matter is often connected to cooling observations of neutron stars: the specific heat in a superfluid is exponentially suppressed, a fact which is consistent with observations of cooling quiescent neutron stars [4]. Furthermore, in the presence of a neutron $^1S_0$ gap, the neutron-neutron bremsstrahlung reaction rate is also suppressed. Cooper-pair breaking/formation neutrino emission processes that occur near the transition temperature are also relevant to the cooling of neutron stars during the crust's thermal relaxation [5,6]. While many of these phenomena are not critically dependent on the magnitude of the gap, recent heat-conduction mechanisms in magnetars require superfluid phonons and their interaction with the lattice ions [7]. These may be more sensitive to the magnitude of the gap.

The neutron matter equation of state [8–17] and pairing gap [18–30] have been the subject of many studies over the years, with quite different results, particularly for the pairing gap. Now, however, cold-atom experiments can mimic the properties of dilute neutron matter, giving nearly direct constraints on its properties. In cold atoms the interaction can be tuned through Feshbach resonances to produce a specific scattering length a, while the effective range r_e between the atoms is nearly zero. In low-density neutron matter, on the other hand, the particle-particle interaction has a scattering length which is very large, ≈ -18.5 fm, much larger than the typical separation between neutrons. The effective range is much smaller than the scattering length, $r_e \approx 2.7$ fm, so $|r_e/a| \approx 0.15$, but only at very low densities is the effective range much smaller than the interparticle spacing. We directly compare results in neutron matter and cold atoms to try to understand the impact of the effective range theoretically; it may also be possible to use narrow and wide resonances in cold atoms to study this experimentally [31].

In a recent article [32], we examined the similarities of cold atoms with neutron matter by calculating the $T = 0$ equations of state and pairing gaps. The interaction used for the cold atoms had an infinitesimal range and the scattering

length was varied to obtain results from $k_F a = -1$ to -10. For the case of neutron matter, we took the s-wave part of the AV18 [33] interaction that fits s-wave nucleon-nucleon scattering very well at both low- and high-energies. In this work, we extend our approach to include p-wave interactions, examining their effects on the equation of state and superfluid pairing gap. Additional corrections due to higher partial waves and three-nucleon interactions are expected to be quite small in this density regime. We also calculate additional properties of neutron matter, including the quasiparticle excitation spectrum, the momentum distribution, and pair-distribution functions.

All calculations are performed using quantum Monte Carlo (QMC) techniques (Sec. III), including variational Monte Carlo (VMC) and Green's function Monte Carlo (GFMC) methods. We compare our results to analytic calculations at very low densities (Sec. II A) and to BCS calculations over the range of densities we consider (Sec. II B). The BCS calculations are also used to try to understand and estimate the finite-size effects in the QMC simulations. Although the BCS results are not expected to be quantitatively accurate, they do provide a useful benchmark for comparisons and for understanding physical effects beyond the mean-field treatment of pairing.

II. ANALYTIC RESULTS

A. Weak coupling

At extremely low densities ($|k_F a| \ll 1$) the effective coupling between neutrons is weak and neutron matter properties can be calculated analytically. The ground-state energy of normal (i.e., nonsuperfluid) matter in this regime was calculated by Lee and Yang in 1957: [34]

$$\frac{E}{E_{\rm FG}} = 1 + \frac{10}{9\pi} k_F a + \frac{4}{21\pi^2}(11 - 2\ln 2)(k_F a)^2, \qquad (1)$$

where $E_{\rm FG}$ is the energy of a free Fermi gas at the same density as the interacting gas. While this expression ignores the contributions of superfluidity, these are exponentially small in $(1/k_F a)$. In the next section we compare these results to QMC calculations for $|k_F a| \geqslant 1$.

The pairing gap at weak coupling is also known analytically. The mean-field BCS approach described below [Eq. (8)] reduces in this limit to:

$$\Delta^0_{\rm BCS}(k_F) = \frac{8}{e^2}\frac{\hbar^2 k_F^2}{2m}\exp\left(\frac{\pi}{2ak_F}\right). \qquad (2)$$

However, as was shown in 1961 by Gorkov and Melik-Barkhudarov [35], the BCS result acquires a finite polarization correction even at weak coupling, yielding a reduced pairing gap:

$$\Delta^0(k_F) = \frac{1}{(4e)^{1/3}}\frac{8}{e^2}\frac{\hbar^2 k_F^2}{2m}\exp\left(\frac{\pi}{2ak_F}\right). \qquad (3)$$

The polarization corrections reduce the mean-field BCS result by a factor of $1/(4e)^{1/3} \approx 0.45$. Interestingly, if one treats the polarization effects at the level of sophistication used in the work of Gorkov and Melik-Barkhudarov, this factor changes with $k_F a$ [36], though there is no *a priori* reason to expect such an approach to be valid at stronger coupling ($k_F a$ of order 1 or more). Calculating the pairing gap in this region has been an onerous task, as can be seen from the multitude of publications devoted to this subject in the past few decades [18–30].

B. BCS in the continuum and in a box

As the coupling strength increases, we expect the BCS mean-field theory to become more accurate. In the BCS-BEC transition studied in cold atoms, the BCS theory goes correctly to the two-body bound state equation in the deep BEC regime. Though we do not expect BCS results to be precise, BCS theory provides a standard basis of comparison for our *ab initio* results and also allows us to analyze finite-size effects in the QMC simulations in a simple way. Within the BCS formalism the wave function is:

$$|\psi\rangle = \prod_{\mathbf{k}}(u_{\mathbf{k}} + v_{\mathbf{k}} c^\dagger_{\mathbf{k}\uparrow} c^\dagger_{-\mathbf{k}\downarrow})|0\rangle, \qquad (4)$$

where $u^2_{\mathbf{k}} + v^2_{\mathbf{k}} = 1$. A variational minimization of the expectation value of the Hamiltonian for an average partice number (or density) leads to the gap equation:

$$\Delta(\mathbf{k}) = -\sum_{\mathbf{k}'}\langle \mathbf{k}|v|\mathbf{k}'\rangle \frac{\Delta(\mathbf{k}')}{2E(\mathbf{k}')}, \qquad (5)$$

where the elementary quasiparticle excitations of the system have energy:

$$E(\mathbf{k}) = \sqrt{\xi(\mathbf{k})^2 + \Delta(\mathbf{k})^2} \qquad (6)$$

and $\xi(\mathbf{k}) = \epsilon(\mathbf{k}) - \mu$, where the chemical potential is μ and $\epsilon(\mathbf{k}) = \frac{\hbar^2 k^2}{2m}$ is the single-particle energy of a particle with momentum $\mathbf{k}$. The chemical potential is found by solving the gap equation together with the equation that provides the average particle number:

$$\langle N\rangle = \sum_{\mathbf{k}}\left[1 - \frac{\xi(\mathbf{k})}{E(\mathbf{k})}\right]. \qquad (7)$$

When interested in the $^1S_0$ gap for neutron matter, it is customary to perform partial-wave expansions of the potential and the gap functions, as well as an angle-average approximation. Thus, Eq. (5) takes the form:

$$\Delta(k) = -\frac{1}{\pi}\int_0^\infty dk' k'^2 \frac{v(k,k')}{E(k')}\Delta(k'), \qquad (8)$$

where the potential matrix element is:

$$v(k,k') = \int_0^\infty dr r^2 j_0(k'r) V(r) j_0(kr). \qquad (9)$$

Similarly, Eq. (7) becomes:

$$\rho = \frac{1}{2\pi^2}\int_0^\infty dk k^2\left[1 - \frac{\xi(k)}{E(k)}\right]. \qquad (10)$$

These equations are one dimensional and thus simple to treat numerically. The density equation can be decoupled from the gap equation only when $\Delta/\mu \ll 1$; this is not the case for the density regime we are considering.

We have solved Eq. (8) in tandem with Eq. (10) for the $^1S_0$ channel of the Argonne v18 [33] potential that contains a strong short-range repulsion. This calculation is greatly simplified if one uses the method described in Ref. [37], thereby transforming the problem into a quasilinear one. We have also solved Eq. (8) together with Eq. (10) for a modified Pöschl-Teller potential:

$$v(r) = -v_0 \frac{2\hbar^2}{m} \frac{\nu^2}{\cosh^2(\nu r)}, \tag{11}$$

where v_0 and ν are parameters which we tuned so that this potential reproduces the neutron-neutron scattering length $a \approx -18.5$ fm and effective range $r_e \approx 2.7$ fm. The potential in Eq. (11) clearly has no repulsive core, making it more amenable to a straightforward iterative solution. In Fig. 1 we show the results for these two potentials. For all the densities considered in this work, the results of solving Eqs. (8) and (10) with these two potentials are virtually indistinguishable. For treatments beyond the mean field, though, more care must be taken. A simple purely attractive interaction with finite positive effective range will produce a collapse to a system size of the range of the potential. The repulsive core avoids this collapse in QMC calculations, but the details of the core interaction are not important at the low densities considered here.

The modified Pöschl-Teller potential can also be used in a calculation for finite average particle number. We have solved Eqs. (5) and (7) for $\langle N \rangle$ from 20 to 200, in periodic boundary conditions in a cubic box of volume L^3:

$$\mathbf{k_n} = \frac{2\pi}{L}(n_x, n_y, n_z). \tag{12}$$

The solution to this problem for many values of $\langle N \rangle$ at a fixed density of $k_F a = -10$ was given in Ref. [32]. There it was found that $\langle N \rangle = 66$ is very close to the thermodynamic limit. We have performed similar calculations for other densities, finding that they all exhibit the same trend. We have also performed similar computations with generalized boundary conditions including separate phase shifts for spin up and down particles at the box boundary [38]. In Fig. 1 we show the results of solving the BCS gap equation Eq. (5) in a periodic box along with the particle-number conserving Eq. (7) for $\langle N \rangle = 66$. We do not expect this procedure to be sufficient for very weak coupling, $|k_F a| < 1$, as the pair size becomes larger than the simulation volume. A more detailed study is warranted to attempt to extract pairing gaps in this regime. In the rest of this work, when we mention BCS results in a box we will refer to the $\langle N \rangle = 66$ case.

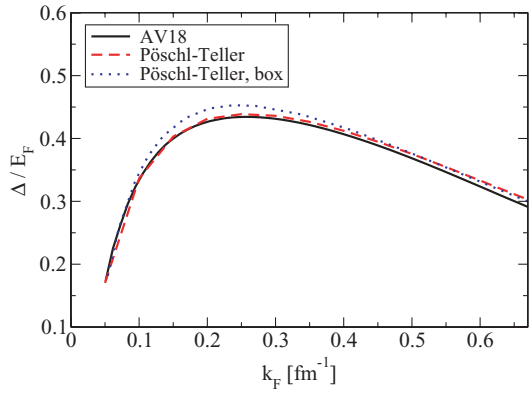

FIG. 1. (Color online) BCS neutron-matter pairing gap Δ divided with the Fermi energy E_F, versus the Fermi momentum k_F for AV18 (solid line) and a modified Pöschl-Teller potential (dashed line) tuned to have the same scattering length and effective range as AV18. At low density the two curves are identical for practical purposes. Also shown is the solution of the BCS problem in a periodic box using the modified Pöschl-Teller potential for 66 particles (dotted line).

We have also calculated, both in the continuum and in a periodic box, the momentum distribution, which in BCS is given by the following expression

$$n(\mathbf{k}) = \frac{1}{2}\left[1 - \frac{\xi(\mathbf{k})}{E(\mathbf{k})}\right], \tag{13}$$

as well as the energy of the quasiparticle excitations, which follows from Eq. (6). These are given in subsections III E and III F.

III. QUANTUM MONTE CARLO

A. Hamiltonian

The Hamiltonian for neutron matter at low densities is:

$$\mathcal{H} = \sum_{k=1}^{N}\left(-\frac{\hbar^2}{2m}\nabla_k^2\right) + \sum_{i<j'} v(r_{ij'}). \tag{14}$$

where N is the total number of particles. The neutron-neutron interaction is generally quite complicated, having one-pion exchange at large distances, an intermediate range spin-dependent attraction by two-pion exchange, and a short-range repulsion. In the regime of interest, though, the scattering length and the effective range are most crucial to the physical properties of the system. For the purposes of our simulation, a short-range repulsive core is also important so as to avoid a collapse to a higher-density state.

In Ref. [32] we used the $^1S_0$ potential as the interaction between all opposite-spin pairs. A perturbative correction was added to correct for the fact that the $S = 1, M_S = 0$ pairs must be in a relative p state (or higher) due to antisymmetry. The p-wave interaction was neglected in those calculations. Here we improve this treatment by explicitly including p-wave interactions in the same-spin pairs and perturbatively correcting the $S = 1, M_S = 0$ pairs to the correct p-wave interaction. We use the AV4 potential to determine the p-wave interactions [39].

The AV4 interaction for neutrons can be simplified to

$$v_4(r) = v_c(r) + v_\sigma(r)\boldsymbol{\sigma}_1 \cdot \boldsymbol{\sigma}_2, \tag{15}$$

which in the case of the $S = 0$ singlet pairs gives

$$v_S(r) = v_c(r) - 3v_\sigma(r). \tag{16}$$

In this article we add the contribution from spin 1 (triplet) pairs:

$$v_P(r) = v_c(r) + v_\sigma(r). \tag{17}$$

The same-spin potential contribution is small even at the highest density considered. While still keeping the potential of Eq. (16) in the propagator of our QMC method for the opposite-spin pairs, we have corrected perturbatively using the general case described in Eq. (15), which can be written as (see, e.g., Ref. [40]):

$$v_4(r) = v_c(r) + v_\sigma(r)(-2P^M - 1) \tag{18}$$

in terms of the Majorana exchange operator.

B. Variational and Green's function Monte Carlo

We employ standard variational and Green's function Monte Carlo methods to calculate the properties of dilute neutron matter. VMC calculations use Monte Carlo integration to minimize the expectation value of the Hamiltonian:

$$\langle H\rangle_{\rm VMC} = \frac{\int d\mathbf{R}\Psi_V(\mathbf{R})H\Psi_V(\mathbf{R})}{\int d\mathbf{R}|\Psi_V(\mathbf{R})|^2} \geqslant E_0. \tag{19}$$

thereby optimizing the variational wave function Ψ_V.

Fixed-node GFMC simulations project out the lowest-energy eigenstate Ψ_0 from a trial (variational) wave function Ψ_V. This they do by treating the Schrödinger equation as a diffusion equation in imaginary time τ and evolving the variational wave function up to large τ.

The ground state is evaluated from:

$$\begin{aligned}\Psi_0 &= \exp[-(H - E_T)\tau]\Psi_V \\ &= \prod \exp[-(H - E_T)\Delta\tau]\Psi_V,\end{aligned} \tag{20}$$

evaluated as a branching random walk. The short-time propagator is usually taken as

$$\exp[-H\Delta\tau] = \exp[-V\Delta\tau/2]\exp[-T\Delta\tau]\exp[-V\delta\tau/2], \tag{21}$$

which is accurate to order $(\Delta\tau)^2$. For the lowest densities considered, we include the two-body propagator exactly:

$$\exp[-H\Delta\tau] = \exp[-T\Delta\tau]\frac{\exp[-H_2\Delta\tau]}{\exp[-H_0\Delta\tau]}, \tag{22}$$

where the two-body Hamiltonian H_2 includes the pair relative kinetic energy and the pair potential and H_0 is the pair kinetic term only. At lowest order in $(\Delta\tau)$ this is equivalent to Eq. (21). However it includes multiple scattering for a pair and allows accurate calculations with larger time steps $\Delta\tau$. This is particularly important for very dilute systems where these multiple-scattering contributions of individual pairs dominate.

The fixed node calculation gives a wave function Ψ_0 that is the lowest-energy state with the sames nodes (surface where $\Psi = 0$) as the trial state Ψ_V. The resulting energy E_0 is an upper bound to the true ground-state energy. The variational wave function Ψ_V has a Jastrow-BCS form (see next subsection) and contains a variety of parameters, many of which affect the nodal surfaces. Since the fixed-node energy is an upper bound to the true ground state, these parameters can be optimized to give the best approximation to the ground-state wave function. In order to optimize these variational parameters, we include them as slowly diffusing coordinates in a preliminary GFMC calculation. The parameters evolve slowly in imaginary time, equilibrating around the lowest-energy state consistent with the chosen form of the trial wave function [41].

The ground-state energy E_0 can be obtained from:

$$E_0 = \frac{\langle\Psi_V|H|\Psi_0\rangle}{\langle\Psi_V|\Psi_0\rangle} = \frac{\langle\Psi_0|H|\Psi_0\rangle}{\langle\Psi_0|\Psi_0\rangle}. \tag{23}$$

Expectation values of quantities that do not commute with the Hamiltonian can be calculated using a combination of the mixed and variational estimate:

$$\langle\Psi_0|\hat{S}|\Psi_0\rangle \approx 2\langle\Psi_0|\hat{S}|\Psi_V\rangle - \langle\Psi_V|\hat{S}|\Psi_V\rangle, \tag{24}$$

where $\hat{S}$ is the operator corresponding to the relevant physical quantity, and the error in this expression is of second order in $\Psi_0 - \Psi_V$. Such a combination of estimates is often called the "extrapolated estimate."

C. Trial wave function

We take the trial wave function to be of the Jastrow-BCS form with fixed particle number:

$$\Psi_V = \prod_{i\neq j} f_P(r_{ij}) \prod_{i'\neq j'} f_P(r_{i'j'}) \prod_{i,j'} f(r_{ij'})\mathcal{A}\left[\prod_{i<j'}\phi(r_{ij'})\right] \tag{25}$$

and periodic boundary conditions. The primed (unprimed) indices correspond to spin-up (spin-down) neutrons. The pairing function $\phi(r)$ is a sum over the momenta compatible with the periodic boundary conditions. In the BCS theory the pairing function is:

$$\phi(r) = \sum_{\mathbf{n}} \frac{v_{\mathbf{k_n}}}{u_{\mathbf{k_n}}} e^{i\mathbf{k_n}\cdot\mathbf{r}} = \sum_{\mathbf{n}} \alpha_n e^{i\mathbf{k_n}\cdot\mathbf{r}}, \tag{26}$$

and here it is parametrized with a short- and long-range part as in Ref. [41]:

$$\phi(\mathbf{r}) = \tilde{\beta}(r) + \sum_{\mathbf{n}, I\leqslant I_C} \alpha_I e^{i\mathbf{k_n}\cdot\mathbf{r}}, \tag{27}$$

where $I = n_x^2 + n_y^2 + n_z^2$ using the parameters defined in Eq. (12). The Jastrow part is taken from a lowest-order-constrained-variational method [42] calculation described by a Schrödinger-like equation:

$$-\frac{\hbar^2}{m}\nabla^2 f(r) + v(r)f(r) = \lambda f(r) \tag{28}$$

for the opposite-spin $f(r)$ and by the corresponding equation for the same-spin $f_P(r)$. Since the $f(r)$ and $f_P(r)$ we get are nodeless, they do not affect the final result apart from reducing the statistical error. The fixed-node approximation guarantees that the result we obtain for one set of pairing function parameters in Eq. (27) will be an upper bound to the true ground-state energy of the system. As in previous works [32,41] the parameters are optimized in the full QMC calculation, providing the best possible nodal surface, in the sense of lowest fixed-node energy, with the given form of trial function. We utilize this upper-bound property to get as close to the true ground-state energy as possible.

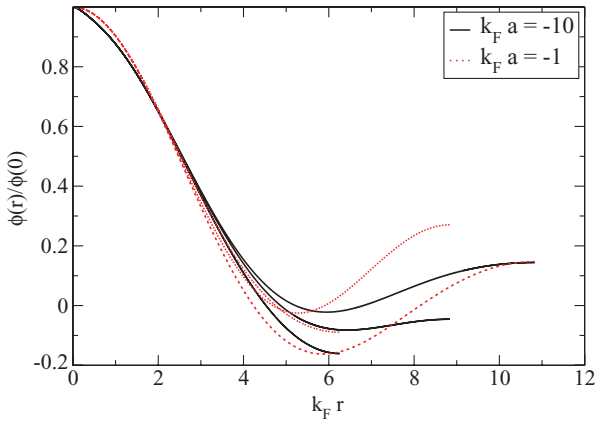

FIG. 2. (Color online) Normalized neutron-matter variationally optimized pairing function $\phi(r)$ for $k_F a = -10$ (solid lines) and $k_F a = -1$ (dotted lines) for different directions in the periodic simulation volume (in terms of rising expanse they correspond to the 001, 011, and 111 directions in the box).

Given the finite-size analysis shown in Refs. [32,38], we have performed all calculations for 66–68 particles in periodic boundary conditions. The equation of state is determined from the 66 particle results, and the pairing gap from the odd-even staggering. We have separately optimized the wave-function parameters at each density and show the results for $\phi(r)$ (normalized each time to the value at zero separation) for the largest and smallest density we have considered ($k_F a = -10$ and $k_F a = -1$) in Fig. 2.

D. Equation of state

We first examine the equation of state of low-density neutron matter, in particular its evolution from the weak- to strong-coupling regime and the impact of adding p-wave interactions between the neutrons. In Fig. 3 we show the equation of state for low-density neutron matter with the s-wave interaction potential along with the new AV4 results. It is clear that when the density is very low, the s-wave

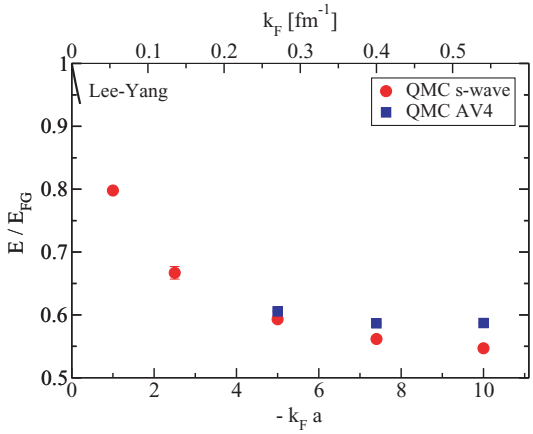

FIG. 3. (Color online) Equation of state for neutron matter using different potentials. Shown are QMC results for the s-wave potential (circles) and for the AV4 (squares). Also shown is the analytic expansion of the ground-state energy of a normal fluid (line).

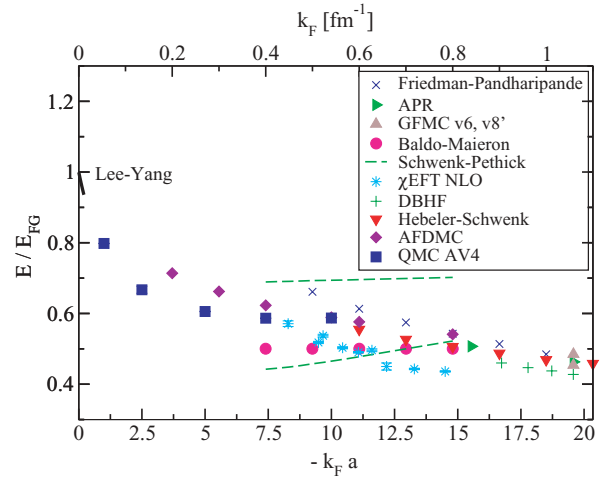

FIG. 4. (Color online) Equation of state for neutron matter compared to various previous results. Despite quantitative discrepancies, all calculations give essentially similar results. Our lowest density corresponds to $k_F a = -1$.

contribution is dominant, and our results for the lowest densities remain unchanged. At higher densities the energy is higher with the contribution of the p-wave interaction. For the highest density examined, $k_F a = -10$, this change is approximately 7%, while for $k_F a = -5$ it is only 1%. Nonperturbative corrections at the highest density considered could reduce the difference between the s-wave interaction and AV4 results slightly. The curve at lower densities shows the analytic result [34] described in subsection II A. Our calculations extend to lower densities than other microscopic calculations and agree with the trend implied by the Lee-Yang result.

We also compare our QMC AV4 results from Fig. 3 for the ground-state energy to other calculations extending to larger Fermi momenta. In Fig. 4 we compare our results to (approximate) variational hypernetted-chain calculations by Friedman and Pandharipande [8] and another calculation by Akmal, Pandharipande, and Ravenhall (APR) [9]. We also include two Green's function Monte Carlo results for 14 neutrons with more complete Hamiltonians [10], a result following from a Brueckner-Bethe-Goldstone expansion [13], a difermion EFT result (shown are the error bands) [11], the latest auxiliary-field diffusion Monte Carlo (AFDMC) result (discussed below) [28], a Dirac-Brueckner-Hartree-Fock calculation [12], a lattice chiral EFT method at next to leading order [14] (see also Ref. [15]), and an approach that makes use of chiral N^{2}LO three-nucleon forces [16]. Of these, Refs. [9], [28], and [16] include a three-nucleon interaction, though at the densities we consider, these are not expected to be significant. Qualitatively all of these results agree within 20%.

A series of *ab initio* calculations for neutron matter using the AFDMC method have been published beginning in 2005 [25]. After our analysis of the finite-size effects—described for BCS in Sec. II B and for QMC in Refs. [32,38]—was published in late 2007, the AFDMC group repeated their calculations for larger systems [28,30], bringing them closer to our results, though still, as can be seen from Fig. 4 the results are distinct.

Given the *ab initio* nature of the powerful AFDMC method, [43] we have attempted to compare results more extensively. The advantage of the AFDMC approach is that it includes an interaction which is more complete than the simpler ones used here. The disadvantage of the AFDMC approach is that it does not provide a variational bound to the energy, and hence the wave functions are chosen from another approach. In the calculations of Refs. [25,28,30] the wave function was taken from a correlated-basis function (CBF) approach that included a BCS-like initial state. The pairing in that variational state is unusually large and in fact increases as a fraction of E_F when the density is lowered.

The QMC AV4 results use a wave function that has been variationally optimized. QMC thus gives energies that are considerably lower than the AFDMC results. As both the wave functions and the interactions are different in the previous QMC and AFDMC results, we have repeated our calculations using the same input wave function [44] used by the AFDMC group (which comes from the same CBF calculation) at $k_F = 0.4$ fm^{-1} and at $k_F a = -10$. We find that in QMC the AV4 results for the optimized wave function [0.5866(6) MeV and 0.5870(3) MeV, respectively] are consistently lower in energy than those using the CBF as input [0.6254(9) MeV and 0.6014(7) MeV, respectively]. This means that they are closer to the true ground-state energy for the Hamiltonian we consider. It would be worth studying in more detail the differences arising from the different Hamiltonians; the most important remaining differences are likely the spin-orbit and pion-exchange terms in the p-wave interaction. Extensions of previous GFMC calculations [10] to lower densities would help to resolve these issues.

It is interesting to note that at the lowest densities considered, the AFDMC and QMC results are still distinct. At those densities contributions of p- and higher partial waves in the Hamiltonian should be very small, and thus the two methods should give identical results. The three-nucleon interaction included in the AFDMC calculations is one possible source of the difference, though this appears unlikely at the smallest densities considered. This suggests that the CBF wave function at very low densities is problematic; additional studies with Jastrow-BCS or other wave functions would be useful.

E. Pairing gap and quasiparticle spectrum

We have also performed calculations for the zero-temperature pairing gap using the AV4 interaction. These follow from our knowledge of the ground-state energy, through the use of the the odd-even staggering formula:

$$\Delta = E(N+1) - \tfrac{1}{2}[E(N) + E(N+2)], \qquad (29)$$

where N is an even number of particles. The results for the gap are shown in Fig. 5. The main conclusion is that the gap remains essentially unchanged with the inclusion of the p-wave interactions. Even at the highest density examined, $k_F a = -10$, the gap is within statistical errors the same comparing s-wave and AV4 interactions. This implies that the dominant contributions to the gap come from the s-wave part of the interaction.

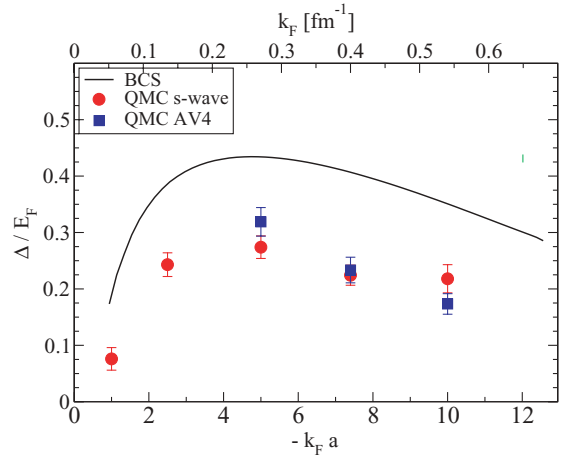

FIG. 5. (Color online) Superfluid pairing gap versus $k_F a$ for neutron matter using different potentials. Shown are QMC results for the s-wave potential (circles) and for the AV4 (squares). Also shown is the mean-field BCS result (line).

Our results indicate that the gap is suppressed by approximately a factor of two from the BCS value at $k_F a = -1$, roughly consistent with the Gorkov and Melik-Barkhudarov, Eq. (3), polarization suppression. In cold atoms, this suppression from BCS is reduced as the density increases, with a smoothly growing fraction of the BCS results as we move from the BCS to the BEC regime. At unitarity the measured pairing gaps [45–47] are 0.45(0.05) of the Fermi energy, for a ratio $\Delta/\Delta_{\rm BCS} \approx 0.65$, in agreement with predictions by QMC methods [32,41,48]. In neutron matter, though, the finite range of the potential reduces Δ/E_F as the density increases. We find a ratio $\Delta/\Delta_{\rm BCS}$ that increases slightly from $|k_F a| = 1$ to 2.5, but thereafter remains roughly constant.

We also used our AV4 calculations to compute the difference between s-wave and AV4 interaction gaps in perturbation theory, in an attempt to isolate the effects of the addition of the p-wave interaction. This perturbation theory may not be accurate for the highest density considered, since the s-wave and AV4 ground states are somewhat different in energy. It should give an accurate picture at lower densities, though, and in particular isolate the sign of the change arising from the p-wave terms in the interaction. Using perturbation theory yields much smaller statistical errors than comparing the separate s-wave and AV4 calculations. Table I shows that the p-wave interactions increase the pairing gap modestly over the range of densities considered. The p-wave interactions apparently decrease the magnitude of the polarization corrections, though the change is only approximately 15% at the highest density considered.

TABLE I. Gap differences at various $k_F a$ calculated in perturbation theory. Perturbative estimates based on AV4 calculations.

$k_F a$	k_F (fm^{-1})	Δ(AV4) (MeV)	Δ(AV4)-$\Delta(s)$ (MeV)
−5.0	0.27	0.48(0.04)	0.012(0.008)
−7.5	0.40	0.77(0.08)	0.11(0.03)
−10.0	0.54	1.05(0.11)	0.16(0.06)

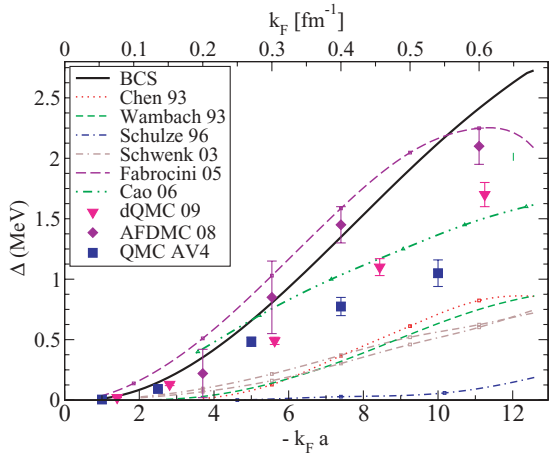

FIG. 6. (Color online) Superfluid pairing gap versus $k_F a$ for neutron matter compared to previous results.

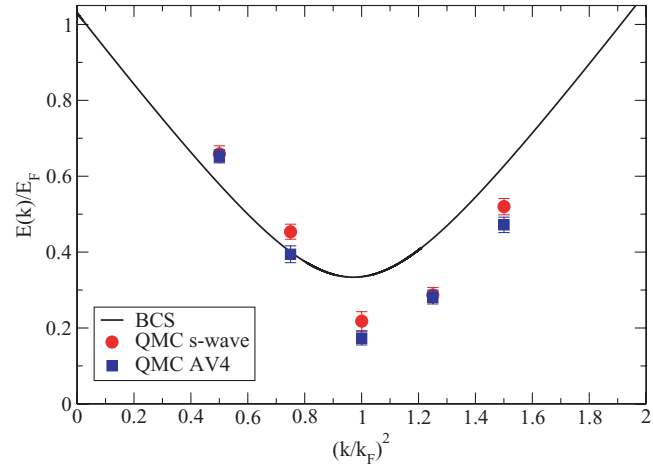

FIG. 7. (Color online) The neutron-matter energy of the quasiparticle excitations of the system in QMC AV4 (squares) versus $(k/k_F)^2$ at $k_F a = -10$. Also shown are the BCS continuum results (line) as well as the QMC quasiparticle spectrum that follows from a simple s-wave Hamiltonian (circles).

In Fig. 6 we compare our results to selected previous results: a CBF calculation by Chen *et al.* [20], an extension of the polarization-potential model by Wambach *et al.* [21], a medium-polarization calculation by Schulze *et al.* [22], a renormalization group calculation by Schwenk *et al.* [23], a Brueckner calculation by Cao *et al.* [26], a determinantal lattice QMC approach [29], and finally the newer CBF calculation by Fabrocini *et al.* [25] that was used as an input wave function in the two AFDMC calculations of 2005 and 2008 [25,28].

The results of our calculations are much larger than most diagrammatic [20–22] and renormalization group [23] approaches. As these approaches assume a well-defined Fermi surface or calculate polarization corrections based on single-particle excitations it is not clear how well they can describe neutron matter in the strongly paired regime or the similar pairing found in cold atoms. Reference [26], which incorporates self-energy corrections and screening at the RPA level within Brueckner theory, appears to give results similar to ours. However, these values disagree with our lower-density results and, perhaps more importantly, at the lowest density reported the gap is larger than the mean-field BCS value (see subsection II A). On a similar note, Refs. [21] and [23] make use of a weak-coupling formula to calculate the pairing gap, similarly to the Eqs. (2) and (3) we discussed in subsection II A. The prefactor they use is justified based on predictions in the theory of ^{3}He. However, the concept itself of a Fermi surface is not well-defined in these strongly paired systems: in ^{3}He, in contrast to the present case, the gap is considerably smaller than the Fermi energy.

Our results are also somewhat different from the AFDMC results of Ref. [28]. We have once again repeated our QMC calculations for the gap using the CBF wave function as input. We find something quite interesting: the QMC method using the AV4 potential and the CBF input wave function at $k_F = 0.4$ fm^{-1} (which gave an energy higher than the variationally optimized input wave function, see subsection III D) gives a gap of 1.21(17) MeV, thus reproducing the AFDMC result, which uses the same input wave function and the much more complicated AV8'+UIX interaction, this being 1.45(15) MeV.

This too suggests that the most important contributions to the gap come from the s-wave part of the interaction. On the other hand, our results seem to qualitatively agree (at least for the lowest densities considered) with a determinantal quantum Monte Carlo lattice calculation [29] which, however, only includes the s-wave component in the interaction. This may imply that a consensus is emerging, in that both these calculations find a gap that is suppressed with respect to the mean-field BCS result but is still a substantial fraction of the Fermi energy. Finally, let us note that, as mentioned before when discussing Fig. 5, the AV4 results for the optimized wave function are very similar to those using an s-wave potential.

We have also calculated the quasiparticle excitation spectrum using the AV4 interaction. The minimum of these results provides the pairing gap in Fig. 5. In Fig. 7 we show both the s-wave Hamiltonian results, as well as the AV4 results. In cold atoms at unitarity and beyond (the BEC regime) the quasiparticle minimum energy is at a momentum significantly smaller than the Fermi momentum. Here, though, the minimum corresponds closely to the neutron Fermi momentum. Although the QMC minimum (pairing gap) is much smaller than the BCS minimum, the dispersion around the minima is quite similar. Just like in the case of cold atoms, microscopic results for the quasiparticle energy spectra [48] can be used to constrain density functional calculations [49].

F. Distribution functions

Using the QMC AV4 interaction, we have also calculated distribution functions. In Fig. 8 we show the momentum distribution at three densities, calculated as the Fourier transform of the one-body density matrix, through:

$$n(k) \equiv \frac{N}{L^3} \left\{ \int d\delta r e^{i\mathbf{k}\cdot(\mathbf{r}'_n - \mathbf{r}_n)} \frac{\Psi_V(\mathbf{r}_1, \ldots, \mathbf{r}'_n)}{\Psi_V(\mathbf{r}_1, \ldots, \mathbf{r}_n)} \right\}, \quad (30)$$

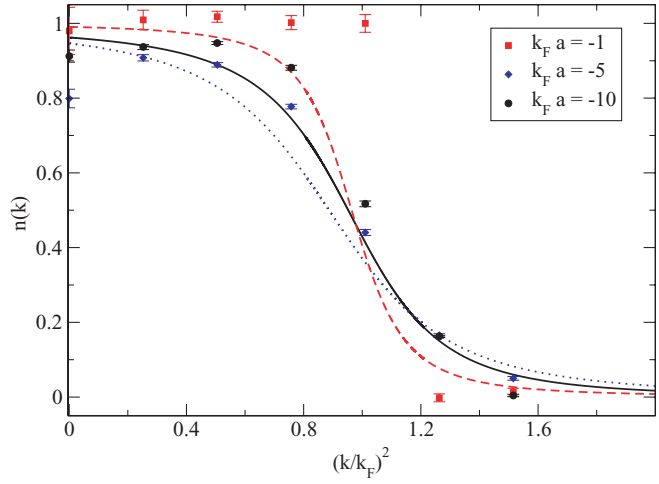

FIG. 8. (Color online) The neutron-matter momentum distribution in QMC versus $(k/k_F)^2$ at $k_F a = -1$ (squares), $k_F a = -5$ (diamonds), and $k_F a = -10$ (circles). Also shown are the continuum BCS results at $k_F a = -1$ (dashed line), $k_F a = -5$ (dotted line), and $k_F a = -10$ (solid line).

where the curly brackets denote a stochastic integration over the angles and we perform the integral over $\delta r = |\mathbf{r}_n' - \mathbf{r}_n|$ on a line using Gaussian quadratures to avoid statistical errors due to the oscillatory radial dependence.

As expected from standard BCS theory, we see that the spread of the momentum distribution around μ is approximately 2Δ. For $k_F a = -1$ the momentum distribution looks very similar to that of a free Fermi gas. At large $|k_F a|$ (when the gap is approximately half the Fermi energy) this fact implies that there is no clearly defined Fermi surface. We note that in Fig. 8 the results for $k_F a = -5$ seems to be more "broadened" than that of $k_F a = -10$, even though as we can see in Fig. 6 the gap at $k_F a = -5$ is considerably smaller than the one at $k_F a = -10$. This is easily resolved if one looks at the pairing gap not in absolute units (MeV) but divided with the Fermi energy, as shown in Fig. 5. The case of $k_F a = -5$ has a bigger gap in units of the Fermi energy, and that is what leads to the observed behavior in the momentum distributions shown in Fig. 8.

We have also computed the pair-distribution functions at $k_F a = -10$ using the AV4 potential and have plotted them in Fig. 9. These are calculated from expectation values of the form:

$$g_P(r) = A \sum_{i<j} \langle \Psi_0 | \delta(r_{ij} - r) O_{ij}^P | \Psi_V \rangle, \qquad (31)$$

where we are initially interested in the case in which the operator is simply unity, and the normalization factor A is such that $g_1(r) \equiv g_c(r)$ goes to one at large distances. These pair-distribution functions provide sum rules related to density- and other response functions versus density and momentum. The solid line in the figure shows the pair-distribution function of noninteracting (NI) fermions with parallel spins:

$$g_c^{NI}(r) = 1 - \frac{9}{(k_F r)^6} [\sin(k_F r) - k_F r \cos(k_F r)]^2 . \qquad (32)$$

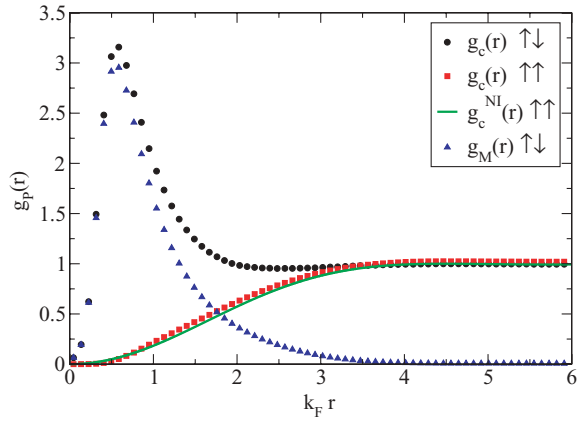

FIG. 9. (Color online) The neutron-matter pair-distribution function in QMC as a function of the distance times the Fermi momentum at $k_F a = -10$. The distribution functions given are the $g_c(r)$ for opposite-spin (circles) and same-spin pairs (squares), as well as the $g_M(r)$ for opposite-spin pairs (triangles).

The noninteracting result is very close to the QMC simulation for same-spin particles. On the other hand, the value of the opposite-spin distribution function is very small at short distances, reflecting the repulsive core in the AV18 potential. Since our interaction is more complicated than a simple s-wave component, Eq. (31) can also be applied to the Majorana exchange operator P^M which was used in Eq. (18). The distribution function for that operator is also shown in Fig. 9 for the density of interest. It tracks the behavior of the central (unit operator) distribution function for short distances but then reduces to approximately half the standard distribution at $k_F r \approx 1.7$.

IV. CONCLUSIONS

To conclude, we have calculated the equation of state and pairing gap of low-density neutron matter with the AV4 interaction from $k_F = 0.054$ to 0.54 fm^{-1}, corresponding to $|k_F a|$ from 1 to 10. The calculated equation of state and pairing gap match smoothly with the known analytic results at low densities and provide important constraints in the strong-coupling regime at large $k_F a$. We have also calculated the quasiparticle spectrum, momentum distribution, and pair-distribution functions for low-density neutron matter. The low-density equation of state can help constrain Skyrme mean-field models of finite nuclei. The pairing gap for low-density neutron matter is relevant to Skyrme-Hartree-Fock-Bogoliubov calculations [3] of neutron-rich nuclei and to neutron-star physics, since it is expected to influence the behavior of the crust [6].

More specifically, a magnetic field in the neutron star crust would have to be approximately 10^{17} G to overcome this gap and thus polarize neutron matter; such a value of the magnetic field is not implausible within the context of magnetars. Similarly, the fact that the magnitude of the gap is not as small as previously expected implies that a new mechanism that makes use of superfluid phonons is competitive to the heat conduction by electrons in magnetized neutron stars [7].

Our results for the gap at the low-density regime, following from a variationally optimized approach that includes the dominant well-known terms in the Hamiltonian, can function as a benchmark with which other calculations can be compared. Equally important, future experimental tests in cold atoms, at least in the very low density regime up to $|k_F a| = 2$ appear to be within the reach of possibility. Similar comparisons may be made with other observables including the pair-distribution function and momentum distribution. We believe that these calculations of the equation of state, pairing gap, and quasiparticle dispersion can be used as constraints of nuclear density functionals.

ACKNOWLEDGMENTS

The authors thank S. Gandolfi, A. Schwenk, and S. Reddy for useful discussions. The work of A.G. and J.C. was supported by the UNEDF SciDAC Collaboration under DOE Grant No. DE-FC02-07ER41457, by the Nuclear Physics Office of the US Department of Energy under Contract No. DE-AC52-06NA25396, and by the LDRD program at Los Alamos National Laboratory. Computing resources were provided at LANL through the Institutional Computing Program and at NERSC. The work of A.G. was supported in part by DOE Grant No. DE-FG02-97ER41014 and by NSF Grant Nos. PHY03-55014 and PHY07-01611.

[1] B. A. Brown, Phys. Rev. Lett. **85**, 5296 (2000).
[2] J. R. Stone, J. C. Miller, R. Koncewicz, P. D. Stevenson, and M. R. Strayer, Phys. Rev. C **68**, 034324 (2003).
[3] N. Chamel, S. Goriely, and J. M. Pearson, Nucl. Phys. **A812**, 72 (2008).
[4] E. F. Brown and A. Cumming, Astrophys. J. **698**, 1020 (2009).
[5] A. W. Steiner and S. Reddy, Phys. Rev. C **79**, 015802 (2009).
[6] D. Page, J. M. Lattimer, M. Prakash, and A. W. Steiner, Astrophys. J. **707**, 1131 (2009).
[7] D. N. Aguilera, V. Cirigliano, J. A. Pons, S. Reddy, and R. Sharma, Phys. Rev. Lett. **102**, 091101 (2009).
[8] B. Friedman and V. R. Pandharipande, Nucl. Phys. **A361**, 502 (1981).
[9] A. Akmal, V. R. Pandharipande, and D. G. Ravenhall, Phys. Rev. C **58**, 1804 (1998).
[10] J. Carlson, J. Morales Jr., V. R. Pandharipande, and D. G. Ravenhall, Phys. Rev. C **68**, 025802 (2003).
[11] A. Schwenk and C. J. Pethick, Phys. Rev. Lett. **95**, 160401 (2005).
[12] J. Margueron, E. van Dalen, and C. Fuchs, Phys. Rev. C **76**, 034309 (2007).
[13] M. Baldo and C. Maieron, Phys. Rev. C **77**, 015801 (2008).
[14] E. Epelbaum, H. Krebs, D. Lee, and U.-G. Meissner, Eur. Phys. J. A **40**, 199 (2009).
[15] E. Epelbaum, H.-W. Hammer, and U.-G. Meissner, Rev. Mod. Phys. **81**, 1773 (2009).
[16] K. Hebeler and A. Schwenk, arXiv:0911.0483 (2009).
[17] A. Rios, A. Polls, and I. Vidaña, Phys. Rev. C **79**, 025802 (2009).
[18] U. Lombardo and H.-J. Schulze, *Lecture Notes in Physics* (Springer-Verlag, Berlin, 2001), Vol. 578, p. 30.
[19] D. J. Dean and M. Hjorth-Jensen, Rev. Mod. Phys. **75**, 607 (2003).
[20] J. M. C. Chen, J. W. Clark, R. D. Davé, and V. V. Khodel, Nucl. Phys. **A555**, 59 (1993).
[21] J. Wambach, T. L. Ainsworth, and D. Pines, Nucl. Phys. **A555**, 128 (1993).
[22] H.-J. Schulze, J. Cugnon, A. Lejeune, M. Baldo, and U. Lombardo, Phys. Lett. **B375**, 1 (1996).
[23] A. Schwenk, B. Friman, and G. E. Brown, Nucl. Phys. **A713**, 191 (2003).
[24] H. Müther and W. H. Dickhoff, Phys. Rev. C **72**, 054313 (2005).
[25] A. Fabrocini, S. Fantoni, A. Y. Illarionov, and K. E. Schmidt, Phys. Rev. Lett. **95**, 192501 (2005).
[26] L. G. Cao, U. Lombardo, and P. Schuck, Phys. Rev. C **74**, 064301 (2006).
[27] J. Margueron, H. Sagawa, and K. Hagino, Phys. Rev. C **77**, 054309 (2008).
[28] S. Gandolfi, A. Yu. Illarionov, S. Fantoni, F. Pederiva, and K. E. Schmidt, Phys. Rev. Lett. **101**, 132501 (2008).
[29] T. Abe and R. Seki, Phys. Rev. C **79**, 054002 (2009).
[30] S. Gandolfi, A. Yu. Illarionov, F. Pederiva, K. E. Schmidt, and S. Fantoni, Phys. Rev. C **80**, 045802 (2009).
[31] B. Marcelis, B. Verhaar, and S. Kokkelmans, Phys. Rev. Lett. **100**, 153201 (2008).
[32] A. Gezerlis and J. Carlson, Phys. Rev. C **77**, 032801(R) (2008).
[33] R. B. Wiringa, V. G. J. Stoks, and R. Schiavilla, Phys. Rev. C **51**, 38 (1995).
[34] T. D. Lee and C. N. Yang, Phys. Rev. **105**, 1119 (1957).
[35] L. P. Gorkov and T. K. Melik-Barkhudarov, JETP **40**, 1452 (1961) [Soviet Phys. JETP **13**, 1018 (1961)].
[36] H.-J. Schulze, A. Polls, and A. Ramos, Phys. Rev. C **63**, 044310 (2001).
[37] V. A. Khodel, V. V. Khodel, and J. W. Clark, Nucl. Phys. **A598**, 390 (1996).
[38] A. Gezerlis, Ph.D. thesis, University of Illinois at Urbana-Champaign, 2009.
[39] R. B. Wiringa and S. C. Pieper, Phys. Rev. Lett. **89**, 182501 (2002).
[40] J. M. Blatt and V. F. Weisskopf, *Theoretical Nuclear Physics* (John Wiley & Sons, New York, 1952).
[41] J. Carlson, S. Y. Chang, V. R. Pandharipande, and K. E. Schmidt, Phys. Rev. Lett. **91**, 050401 (2003).
[42] V. R. Pandharipande and H. A. Bethe, Phys. Rev. C **7**, 1312 (1973).
[43] K. E. Schmidt and S. Fantoni, Phys. Lett. **B446**, 99 (1999).
[44] S. Gandolfi (private communication, 2009).
[45] Y. Shin, C. H. Schunck, A. Schirotzek, and W. Ketterle, Nature **451**, 689 (2008).
[46] J. Carlson and S. Reddy, Phys. Rev. Lett. **100**, 150403 (2008).
[47] A. Schirotzek, Y. I. Shin, C. H. Schunck, and W. Ketterle, Phys. Rev. Lett. **101**, 140403 (2008).
[48] J. Carlson and S. Reddy, Phys. Rev. Lett. **95**, 060401 (2005).
[49] A. Bulgac and Michael McNeil Forbes, Phys. Rev. Lett. **101**, 215301 (2008).